Multi-scale Opening – A New Morphological Operator

Subhadip Basu[1(✉)], Eric Hoffman[2], and Punam K. Saha[2,3]

[1] Department of Computer Science and Engineering, Jadavpur University, Kolkata 700032, India
subhadip@cse.jdvu.ac.in
[2] Department of Radiology and the Department of Biomedical Engineering, The University of Iowa, Iowa City, IA 52242, USA
eric-hoffman@uiowa.edu
[3] Department of Electrical and Computer Engineering, The University of Iowa, Iowa City, IA 52242, USA
pksaha@engineering.uiowa.edu

Abstract. Theoretical properties of multi-scale opening (MSO), a new mathematical morphological operator, are established and its application to separation of conjoined fuzzy objects is presented. The new MSO operator accounts for distinct intensity properties of individual objects inside the assembly of two conjoined fuzzy objects by combining fuzzy distance transform (FDT), a morphologic feature, with fuzzy connectivity, a topologic feature, to iteratively open two objects starting at large scales and progressing toward finer scales. Results of application of the new mathematical morphological operator to separate conjoined arterial structures in mathematically generated phantoms and for segmentation of arteries and veins in a physical cast phantom of a pig lung are presented. Performance of the MSO operator is also evaluated in terms of patients' pulmonary non-contrast CT data for separating arteries and veins and for complete carotid vascular segmentation for patient's CTA data set.

Keywords: Fuzzy distance transform · Morphology · Multi-scale opening

1 Introduction

Knowledge extraction over varying scales or multiple layers in two- and higher-dimensional images has remained a front-line research objective over several decades [1–5]. Object segmentation in images is one of the major challenges in many such applications[6–11]. It is difficult to design general purpose segmentation methods and, often, we face a new segmentation challenge that may not be efficiently solved the using existing methods. Design of the mathematical morphological operators play a key role in the success of many segmentation methods. In case of multi-layered extraction of knowledge, the segmentation results are often found to be extremely sensitive to the choice of the structure size of the morphological operators. In this work, we present multi-scale opening (MSO) as a new mathematical morphological operator, capable of separating two conjoined fuzzy objects over varying scales. We also present the theoretical validations for the new morphological operator and

V. Murino and E. Puppo (Eds.): ICIAP 2015, Part II, LNCS 9280, pp. 417–427, 2015.
DOI: 10.1007/978-3-319-23234-8_39

present the results with respect to both mathematical and vessel-cast phantoms and patients' data. Two different situations may arise here regarding the intensity distribution of the conjoined structures, 1) segmentation of fused iso-intensity objects and, 2) segmentation in shared intensity space.

The developed MSO operator use fuzzy distance transform (FDT) [16], a morphologic feature, with topologic fuzzy connectivity [17–20] algorithm to develop a multi-scale opening operator for separating two conjoined fuzzy objects fused at different locations and scales. The proposed method for multi-scale opening starts with a fuzzy segmentation of the assembly of two conjoined objects, and two sets of seed points (one for each object). The method outputs spatially separated objects. It is designed under the assumption that fusions of the two objects are locally separable using a suitable morphological opening operator. The method uses a novel approach to solve the following two fundamental challenges: 1) how to find local size of morphological operators and, 2) how to trace continuity of locally separated regions. These challenges are met by combining FDT, a morphologic feature with a topologic fuzzy connectivity, and a constrained dilation to iteratively open finer and finer details starting at large scales and progressing toward smaller scales.

2 Theory of Multi-Scale Opening of Conjoined Fuzzy Objects

A three dimensional (3D) cubic grid, is represented by $\mathcal{Z}^3|$ $\mathcal{Z}$ is the set of integers. A grid point, often referred to as a point or a voxel, is an element of $\mathcal{Z}^3$ and is represented by a triplet of integer coordinates. Standard 26-adjacency [21] is used here, i.e., two voxels $p = (x_1, x_{2,} x_3), q = (y_1, y_{2,} y_3) \in \mathcal{Z}^3$ are adjacent if and only if $\max_{1\leq i\leq 3}|x_i - y_i| \leq 1$, where $|\cdot|$ returns the absolute value. Two adjacent voxels are often referred to as neighbors of each other; the set of 26-neighboors of a voxel p excluding itself is denoted by $\mathcal{N}^*(p)$. An object $\mathcal{O}$ is a fuzzy set $\{(p, \mu_{\mathcal{O}}(p))|p \in \mathcal{Z}^3\}$ of $\mathcal{Z}^3$, where $\mu_{\mathcal{O}}: \mathcal{Z}^3 \rightarrow [0,1]$ is the membership function. The support $\Theta(\mathcal{O})$ of an object $\mathcal{O}$ is the set of all voxels with non-zero membership, i.e., $\Theta(\mathcal{O}) = \{p \mid p \in \mathcal{Z}^3 \text{ and } \mu_{\mathcal{O}}(p) \neq 0\}$; $\bar{\Theta}(\mathcal{O}) = \mathcal{Z}^3 - \Theta(\mathcal{O})$ is the background. Images are always acquired with a finite field of view. Thus, we will assume that an object always has a bounded support. Let S denote a set of voxels; a path π in S from $p \in S$ to $q \in S$ is a sequence $\langle p = p_1, p_2, \cdots, p_l = q\rangle$ of voxels in S such that every two successive voxels on the path are adjacent. A link is a path $\langle p, q\rangle$ consisting of exactly two mutually adjacent voxels $p, q \in \mathcal{Z}^3$. The length of a path $\pi = \langle p_1, p_2, \cdots, p_l\rangle$ in a fuzzy object $\mathcal{O}$, denoted by $\Pi_{\mathcal{O}}(\pi)$, is defined as the sum of lengths of all links along the path, i.e.,

$$\Pi_{\mathcal{O}}(\pi) = \sum_{i=1}^{l-1} \frac{1}{2}\left(\mu_{\mathcal{O}}(p_i) + \mu_{\mathcal{O}}(p_{i+1})\right) \| p_i - p_{i+1} \|. \quad (1)$$

The *fuzzy distance* between two voxels $p, q \in \mathcal{Z}^3$ in an object $\mathcal{O}$, denoted by $\omega_{\mathcal{O}}(p,q)$, is the length of one of the shortest paths from p to q, i.e.,

$$\omega_{\mathcal{O}}(p,q) = \min_{\pi \in \mathcal{P}(p,q)} \Pi_{\mathcal{O}}(\pi) |\, \mathcal{P}(p,q), \tag{2}$$

where, $\mathcal{P}(p,q)$ is set of all paths from p to q. The *fuzzy distance transform* or *FDT* of an object $\mathcal{O}$ is an image $\{(p, \Omega_{\mathcal{O}}(p)) |\, p \in \mathcal{Z}^3\}$, where $\Omega_{\mathcal{O}}: \mathcal{Z}^3 \rightarrow \Re^+ |\, \Re^+$ is set of positive real numbers including zero, is the fuzzy distance from background. i.e.,

$$\Omega_{\mathcal{O}}(p) = \min_{q \in \bar{\Theta}(\mathcal{O})} \omega_{\mathcal{O}}(p,q). \tag{3}$$

Local scale is defined as the depth (i.e., the FDT value) at the nearest locally-deepest voxels. Let $S_{\max} \subset \Theta(\mathcal{O})$ be the set of locally-deepest voxels, i.e., $S_{\max} = \{p \mid p \in \Theta(\mathcal{O})$ and $\forall q \in \mathcal{N}_l(p),\ \Omega_{\mathcal{O}}(q) \leq \Omega_{\mathcal{O}}(p)\}$, where $\mathcal{N}_l(p)$ is the $(2l+1)^3$ neighborhood of p; here, $\mathcal{N}_2(p)$ is used to avoid noisy local maxima. Local scale at a voxel p, denoted by $\delta_{\mathcal{O}}(p)$, is defined as the FDT value of the voxel in $S_{\max}$ nearest to p. Now onward, both "FDT" and $\Omega_{\mathcal{O}}$ will refer to "scale-normalized FDT".

Let us assume two fuzzy objects $\mathcal{O}_{\mathcal{A}}$ and $\mathcal{O}_{\mathcal{B}}$, which are fused at various unknown locations and scales. The segmentation of the two fuzzy objects is solved using a new MSO operator in two sequential steps – Step 1: segmentation of the combined region $\mathcal{O}_{\mathcal{A}} \cup \mathcal{O}_{\mathcal{B}}$ from the background, and Step 2: separation of $\mathcal{O}_{\mathcal{A}}$ and $\mathcal{O}_{\mathcal{B}}$. The first step may trivially be achieved using simple thresholding [22, 23] and connectivity analysis [24, 25]. Let $\mathcal{O}$ be the fuzzy segmentation of the combined region obtained in Step 1. All subsequent analyses will be confined to the support $\Theta(\mathcal{O})$ of $\mathcal{O}$; let $I: \Theta(\mathcal{O}) \rightarrow [I_{\min}, I_{\max}]$ be image intensity function over $\Theta(\mathcal{O})$.

In the second step, segmentation is modeled as opening of two fuzzy objects mutually fused at different unknown regions and scales. Often, a simple fuzzy connectivity or edge analysis may not be suitable to separate the two structures. On the other hand, the two objects may frequently be locally separable using a suitable morphological opening operator. The challenges here are – (1) how to determine local size of suitable morphological operators and (2) how to combine the locally separated regions. The MSO operator combines fuzzy distance transform (FDT) [26], [16] a morphologic function with a topologic fuzzy connectivity [17, 18, 27] to iteratively open the two objects starting at large scales and progressing toward finer scales.

2.1 Optimal Erosion Using Morpho-Connectivity

Here, we define the algorithm during the first iteration. It starts with two sets of seed voxels $S_{\mathcal{A}}$ and $S_{\mathcal{B}}$ and a set of common separators $S_{\mathcal{S}}$. The initial FDT map $\Omega_{\mathcal{A},0}$ for the first object is computed from $\mathcal{O}$ except that the voxels in $S_{\mathcal{B}} \cup S_{\mathcal{S}}$ are added to the background; it is worth mentioning that the local scale map $\delta_{\mathcal{O}}$, derived from the original assembled object $\mathcal{O}$, is used for normalization. FDT map $\Omega_{\mathcal{B}}$ for the other object is computed similarly. It is reasonable to assume that the sets $S_{\mathcal{A}}$, $S_{\mathcal{B}}$, and $S_{\mathcal{S}}$ are mutually exclusive.

Fuzzy morpho-connectivity strength of a path $\pi = \langle p_1, p_2, \cdots, p_l \rangle$ in a fuzzy object $\mathcal{O}$, denoted as $\Gamma_{\mathcal{O}}(\pi)$, is the minimum FDT value along the path:

$$\Gamma_{\mathcal{O}}(\pi) = \min_{1 \le i \le l} \Omega_{\mathcal{O}}(p_i) \ . \tag{4}$$

Fuzzy morpho-connectivity between two voxels $p, q \in \mathcal{Z}^3$, denoted as $\gamma_{\mathcal{O}}(p, q)$, is the strength of one of the strongest morphological paths between p and q, i.e.,

$$\gamma_{\mathcal{O}}(p, q) = \max_{\pi \in \mathcal{P}(p,q)} \Gamma_{\mathcal{O}}(\pi). \tag{5}$$

Definition 2.1. Optimum erosion for a fuzzy object $\mathcal{A}$ represented by the set of seed voxels $S_{\mathcal{A}}$ with respect to its co-object $\mathcal{B}$ represented by the set of seed voxels $S_{\mathcal{B}}$ and a set of common separator S_S is the set of all voxels p such that there exists an erosion scale that disconnects p from $\mathcal{B}$ while leaving it connected to $\mathcal{A}$, i.e.,

$$R_{\mathcal{A},0} = \left\{ p \mid \max_{a \in S_{\mathcal{A}}} \gamma_{\mathcal{A},0}(a, p) > \max_{b \in S_{\mathcal{B}}} \gamma_{\mathcal{B},0}(b, p) \right\}, \tag{6}$$

where, the fuzzy morpho-connectivity functions $\gamma_{\mathcal{A},0}$ and $\gamma_{\mathcal{B},0}$ are defined from the FDT maps $\Omega_{\mathcal{A},0}$ and $\Omega_{\mathcal{B},0}$, respectively The optimum erosion $R_{\mathcal{B},0}$ for the object $\mathcal{B}$ is defined similarly.

Proposition 2.1. For any fuzzy object $\mathcal{O}$ in $\mathcal{Z}^3$, for any two mutually exclusive sets of seeds $S_{\mathcal{A}}$ and $S_{\mathcal{B}}$, representing two different objects, and a set of common separator S_S disjoint to both $S_{\mathcal{A}}$ and $S_{\mathcal{B}}$, the separated regions $R_{\mathcal{A},0}$, $R_{\mathcal{B},0}$, after optimum erosion, are always disjoint, i.e., $R_{\mathcal{A},0} \cap R_{\mathcal{B},0} = \emptyset$.

Proof. To prove this proposition by contradiction, let us assume that the proposition is not true, i.e., $R_{\mathcal{A},0} \cap R_{\mathrm{B},0} \neq \emptyset$. Let us consider a voxel p in $R_{\mathcal{A},0} \cap R_{\mathrm{B},0}$ and from Eqn. (6) the voxel p belongs to $R_{\mathcal{A},0}$ since, $\max_{a \in S_{\mathcal{A}}} \gamma_{\mathcal{A},0}(a, p) > \max_{b \in S_{\mathcal{B}}} \gamma_{\mathcal{B},0}(b, p)$. But since the voxel p also belongs to $R_{\mathrm{B},0}$, following the same equation, $\max_{b \in S_{\mathcal{B}}} \gamma_{\mathcal{B},0}(b, p) > \max_{a \in S_{\mathcal{A}}} \gamma_{\mathcal{A},0}(a, p)$. Hence contradiction. ▪

2.2 Constrained Dilation

The two optimally eroded regions $\mathrm{R}_{\mathcal{A},0}$ and $\mathrm{R}_{\mathcal{B},0}$ (Fig. 1(a)) separates the two target objects using morpho-connectivity. However, each of these two separated regions captures only an eroded version of the target objects over respective local regions and dilation is needed to further improve the delineation results (Fig. 1(b)). Also, the annular left-over of optimal erosion (Fig. 1(a)) wrongly permits path leakages from one separated region into the other. It is crucial to block such leakages in order to proceed with the separation process to the next finer scale. Both objectives are fulfilled by local dilation of the two separated objects and we refer to it as a "constrained dilation" Constrained dilation is applied over a "morphological neighborhood" to ensure that the dilation is locally confined.

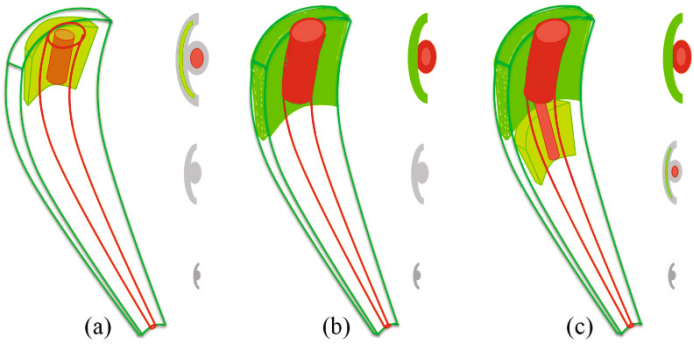

Fig. 1. A schematic illustration of the results of different steps in the MSO algorithm – (a) optimal erosion, (b) constrained dilation, and (c) iterative progression to the next iteration.

Definition 2.2. Morphological neighborhood of a set of voxels X in an object $\mathcal{O}$, denoted by $N_{\mathcal{O}}(X)$, is a set of all voxels $p \in \Theta(\mathcal{O})$ such that $\exists\, q \in X$ for which $\omega_{\mathcal{O}}(p,q) < \Omega_{\mathcal{O}}(q)$ and p is connected to q by a path $\pi = \langle p = p_1, p_2, \cdots, p_l = q \rangle$ of monotonically increasing FDT values.

To define morphological neighborhood, original FDT map without scale normalization is used as morphological neighborhood should capture original un-normalized scale and geometry of the local structure.

Definition 2.3. *Constrained dilation* of $R_{\mathcal{A},0}$ with respect to its co-object $R_{\mathcal{B},0}$ within the fuzzy object $\mathcal{O}$, denoted as $M_{\mathcal{A},0}$, is the set of all voxels $p \in N_{\mathcal{O}}(R_{\mathcal{A},0})$ which are strictly closer to $R_{\mathcal{A},0}$ than $R_{\mathcal{B},0}$ (Fig. 1(b)), i.e.,

$$M_{\mathcal{A},0} = \left\{ p \mid p \in N_{\mathcal{O}}\left(R_{\mathcal{A},0}\right) \wedge \max_{a \in R_{\mathcal{A},0}} \omega_{\mathcal{O}}(a,p) > \max_{b \in R_{\mathcal{B},0}} \omega_{\mathcal{O}}(b,p) \right\}, \qquad (7)$$

where, the fuzzy distance function $\omega_{\mathcal{O}}$ is defined over the fuzzy object $\mathcal{O}$ in $\mathcal{Z}^3$. The region $M_{\mathcal{B},0}$ is defined similarly.

It may be noted that, gaps between the separated regions visible in Fig. 1(a) are filled in Fig. 1(b) after constrained dilation and, thus, undesired paths running through those gaps are blocked enabling separation at the next finer scale. The two steps of optimal erosion and constrained dilation lead to an "optimal opening" operation preparing the ground for separation at next finer scales.

Proposition 2.2. For any fuzzy object $\mathcal{O}$ in $\mathcal{Z}^3$, for any two mutually exclusive sets of seeds $S_{\mathcal{A}}$ and $S_{\mathcal{B}}$, representing two different objects, and a set of common separator $S_{\mathcal{S}}$ disjoint to both $S_{\mathcal{A}}$ and $S_{\mathcal{B}}$, the constrained dilations $M_{\mathcal{A},0}$ $M_{\mathcal{B},0}$ are always disjoint, i.e., $M_{\mathcal{A},0} \cap M_{\mathcal{B},0} = \emptyset$.

Proof. To prove this proposition by contradiction first let us assume that the proposition is not true, i.e., $M_{\mathcal{A},0} \cap M_{\mathcal{B},0} \neq \emptyset$. Let us consider a voxel p in $M_{\mathcal{A},0} \cap M_{\mathcal{B},0}$.

Following $p \in M_{\mathcal{A},0}$ and *Definition 2.3*, we have $\max_{a \in R_{\mathcal{A},0}} \omega_{\mathcal{O}}(a,p) > \max_{b \in R_{\mathcal{B},0}} \omega_{\mathcal{O}}(b,p)$. Therefore p is strictly closer to $R_{\mathcal{A},0}$. But since p also belongs to $M_{\mathcal{B},0}$, following *Definition 2.3*, we have $\max_{a \in R_{\mathcal{B},0}} \omega_{\mathcal{O}}(a,p) > \max_{b \in R_{\mathcal{A},0}} \omega_{\mathcal{O}}(b,p)$, making p strictly closer to $R_{\mathcal{B},0}$ as well. But from *Proposition 2.1* we have, $R_{\mathcal{A},0} \cap R_{\mathcal{B},0} = \emptyset$. Therefore the voxel p cannot be strictly closer to both $R_{\mathcal{A},0}$ and $R_{\mathcal{B},0}$ simultaneously. Hence contradiction. ▪

2.3 Iterative Progression to Multi-Scale Opening

The optimal opening algorithm, as described above, separates two target objects at a specific scale and the purpose of the current step is to freeze the boundary of previous separation enabling propagation to the next finer scale. This step operates in a fashion similar to the iterative strategy described in references [19, 28] for intensity based fuzzy connectivity. For each of the two objects, we set the FDT values to zero over the region currently acquired by its rival object. Specifically, after each iteration, the FDT image of object $\mathcal{A}$ is updated as follows:

$$\Omega_{\mathcal{A},i}(p) = \begin{cases} 0, & \text{if } p \in N_{\mathcal{O}}\left(R_{\mathcal{B},i-1}\right) - M_{\mathcal{A},i-1}, \\ \Omega_{\mathcal{O},i-1}(p), & \text{otherwise}. \end{cases} \tag{8}$$

The FDT map of the other object is updated similarly. The seed voxels $S_{\mathcal{A}}$ and $S_{\mathcal{B}}$ for the two objects are replaced by $M_{\mathcal{A},i-1}$ and $M_{\mathcal{B},i-1}$, respectively (Fig. 1(c)). Then, the morphological separations $M_{\mathcal{A},i}$ and $M_{\mathcal{B},i}$ are derived using the Eqns. (6-8) and *Definition 2.1* to *Definition 2.3*.

Proposition 2.3. For any fuzzy object $\mathcal{O}$ in $\mathcal{Z}^3$, for any two mutually exclusive sets of seeds $S_{\mathcal{A}}$ and $S_{\mathcal{B}}$, representing two different objects, and a set of common separator S_S disjoint to both $S_{\mathcal{A}}$ and $S_{\mathcal{B}}$, for any positive integer i, the separation results $M_{\mathcal{A},i}$, $M_{\mathcal{B},i}$ of the MSO algorithm are always disjoint, i.e., $M_{\mathcal{A},i} \cap M_{\mathcal{B},i} = \emptyset$.

Proof. This proposition will be proved by induction. From *Proposition 2.1* we have $R_{\mathcal{A},0} \cap R_{\mathcal{B},0} = \emptyset$ and from *Proposition 2.2* we have $M_{\mathcal{A},0} \cap M_{\mathcal{B},0} = \emptyset$. This ensures disjoint separation of the two fuzzy objects after the first iteration of the MSO algorithm. Let us assume that this proposition is true after $(i-1)^{\text{th}}$ iteration, for some $i > 1$. To complete the proof, we will show that the proposition remains true after the i^{th} iteration. During the i^{th} iteration of multi-scale opening, the following changes take place in the optimum erosion and iterative progression steps as compared to the first iteration: $\Omega_{\mathcal{A},0}$ (or, $\Omega_{\mathcal{B},0}$) is replaced by $\Omega_{\mathcal{A},i}$ (respectively, $\Omega_{\mathcal{B},i}$) in Equation (6) and the set seeds $S_{\mathcal{A}}$ is replaced by $M_{\mathcal{A},i-1}$ instead of $M_{\mathcal{A},0}$ while $S_{\mathcal{B}}$ is replaced by $M_{\mathcal{B},i-1}$, instead of $M_{\mathcal{B},0}$. Therefore, following *Proposition 2.1* and *Proposition 2.3*, the results of optimum erosion and constrained dilation, the output separation of the i^{th} iteration remain disjoint, i.e., $M_{\mathcal{A},i} \cap M_{\mathcal{B},i} = \emptyset$. ▪

Proposition 2.4. For any fuzzy object $\mathcal{O}$ in $\mathcal{Z}^3$, for any two mutually exclusive sets of seeds $S_{\mathcal{A}}$ and $S_{\mathcal{B}}$, representing two different objects, and a set of common separator S_S disjoint to both $S_{\mathcal{A}}$ and $S_{\mathcal{B}}$, for any positive integer i, the separation results $M_{\mathcal{A},i} \subset M_{\mathcal{A},i+1}$.

Proof. Following iterative progression of multi-scale opening, during the $(i+1)^{\text{th}}$ iteration, $M_{\mathcal{A},i}$ is used as the set of seeds for the object $\mathcal{A}$. Following *Definition 2.3*, $M_{\mathcal{A},i} \subset N_{\mathcal{O}}(R_{\mathcal{A},i})$; following *Proposition 2.3,* $M_{\mathcal{A},i} \cap M_{\mathcal{B},i} = \emptyset$. Therefore, $p \in M_{\mathcal{A},i} \subset M_{\mathcal{A},i} - M_{\mathcal{B},i} \subset N_{\mathcal{O}}\left(R_{\mathcal{A},i}\right) - M_{\mathcal{B},i}$. Thus, following Equation (8), $\forall p \in M_{\mathcal{A},i}$, $\Omega_{\mathcal{B},i+1}(p) = 0$. Hence, following Equation (6), $M_{\mathcal{A},i} \subset R_{\mathcal{A},i+1} \subset M_{\mathcal{A},i+1}$. ▪

Proposition 2.5. For any fuzzy object $\mathcal{O}$ in $\mathcal{Z}^3$ with a finite support $\Theta(\mathcal{O})$, for any two mutually exclusive sets of seeds $S_{\mathcal{A}}$ and $S_{\mathcal{B}}$, representing two different objects, and a set of common separator S_S disjoint to both $S_{\mathcal{A}}$ and $S_{\mathcal{B}}$, the MSO algorithm terminates in a finite number of iterations.

Proof. For all voxels, $p \in \bar{\Theta}(\mathcal{O})$, for any $i \geq 0$, the FDT maps $\Omega_{\mathcal{A},i}(p) = \Omega_{\mathcal{B},i}(p) = 0$. Therefore, following Eqn. (6), $R_{\mathcal{A},i}, R_{\mathcal{B},i} \subset \bar{\Theta}(\mathcal{O})$. Following *Definition 2.2*, the morphological neighborhoods $N_{\mathcal{O}}\left(R_{\mathcal{A},i}\right), N_{\mathcal{O}}(R_{\mathcal{B},i}) \subset \bar{\Theta}(\mathcal{O})$. Therefore, the results of constrained dilation $M_{\mathcal{A},i}$ and $M_{\mathcal{B},i}$ are confined to the finite set. Again, following *Proposition 2.4*, $M_{\mathcal{A},i}$ and $M_{\mathcal{B},i}$ are monotonically non-contracting. Therefore, after a finitely many iterations, both these sets converge when MSO algorithm terminates. ▪

3 Experimental Results

In this section, we describe our experimental plans, methods, and qualitative results to examine the accuracy of segmentation results with the MSO operator, both in isointesity and shared intensity space. Performance of the system is first evaluated on two different types of phantom images, 1) conjoined mathematical phantoms in iso-intensity space, 2) CT images of a pig pulmonary vessel cast phantom with contrast separated A/V trees in shared intensity space. Another experiment is conducted on two different sets of patients' data, i.e., 1) pulmonary non-contrast CT data for separating arteries and veins in iso-intensity space and, 2) for complete carotid vascular segmentation for patient's CTA data in shared intensity space.

At first, four mathematical phantoms are computer-generated where each phantom is an assembly of two cylindrical objects running quasi-parallel across the slice direction with different geometry and varying levels of fuzziness, overlap, scale and noise. These phantom images were initially generated at high resolution after assigning a pure intensity values for the two structures. Subsequently, each of these images was down sampled using $3 \times 3 \times 3$ window to simulate partial volume effects. Each down-sampled image was further degraded with additive white Gaussian noise at SNR of 12. Using a graphical user interface, exactly one seed point was placed for

each object near its center on the top-most slice at the largest-scale level. Fig. 2 shows that, even in the presence of significant overlap, down sampling and random noise, the method can separate the two conjoined structures. Note that the method of multi-scale opening has successfully removed the partial volume effects.

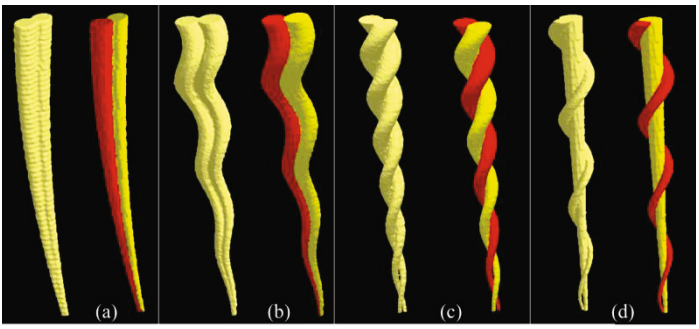

Fig. 2. Results of application of the MSO operator on four computer-generated phantoms after 3x3x3 down-sampling are shown. Each block shows the original phantom (left) of two mutually fused objects and the color-coded results of the separation using the multi-scale opening operator.

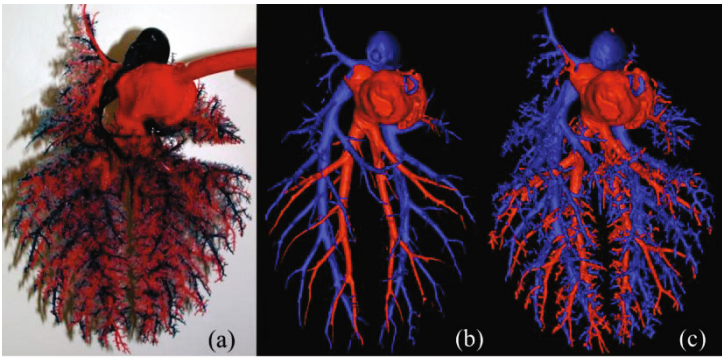

Fig. 3. Results of artery/vein (A/V) separation on a pulmonary pig vessel cast phantom are shown. (a) Photograph of the phantom. (b) 3-D rendering of the optimum thresholding result. (c) 3-D rendering of the A/V separation results using the MSO algorithm.

Results of application of the algorithm to a CT image of a pig lung cast phantom with different CT contrasts for arterial and venous trees are presented in Fig. 3. The vessel cast was scanned on a Siemens Somatom Definition Flash 128 CT scanner using the following protocol – 120 kV, 115 effective mAs, 1-s rotation speed, pitch factor: 1.0, nominal collimation: 16 mm × 0.3 mm, image matrix: 512 × 512 and (0.34 mm)2 in-plane resolution, and 0.75 mm slice thickness. Two CT intensity values $I_{\min}$ and I_{artery} segmenting the background and pure artery regions were manually selected by three independent users. Therefore, the intensity range $[I_{\min}, I_{\text{artery}}]$ was used as the shared intensity space. The superiority of the new MSO

operator lies in its ability to trace fine structures of individual objects despite the presence of partial voluming and intensity sharing. For this experiment, two seed voxels were used for arteries and another three seed voxels were used for veins using our custom 2D/3D graphical interface.

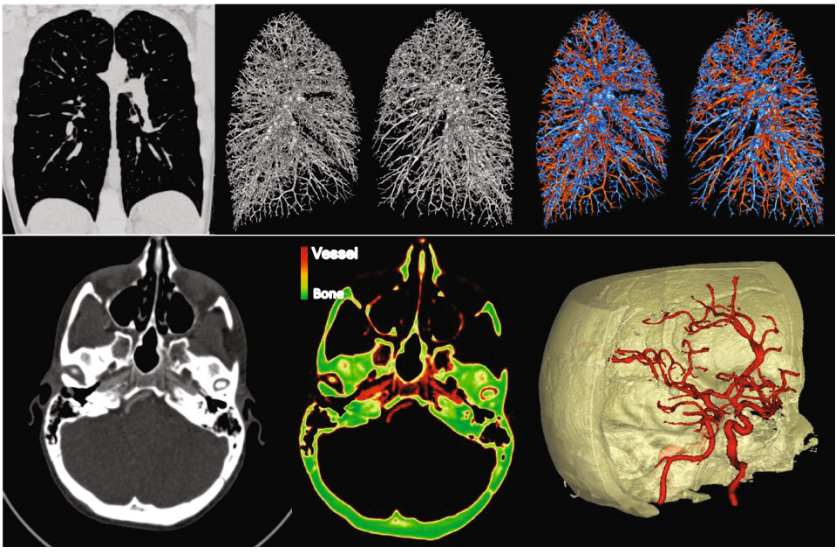

Fig. 4. Results of applying the MSO operator on patients' data. (top) artery/vein separation on a pulmonary non-contrast CT data, (bottom) carotid vessel segmentation in a patient's CTA data.

The effectiveness of the MSO operator has also been examined qualitatively on clinical pulmonary multidetector CT images. A result of application of the method separating pulmonary arteries/veins in a non-contrast thoracic CT image of a healthy subject is qualitatively illustrated in Fig. 4 (top row). The thoracic region of the patient is imaged using a Siemens Sensation 64 multidetector CT scanner at 120 kVp and 100 mA. The subject was scanned in feet-first supine position. The image was acquired at 0.75 mm slice thickness and was reconstructed with 0.5 mm slice thickness and in-plane resolution. 25-30 seed points for each of the arteries and veins were manually selected by an expert using a 2-D-slice-display graphical interface followed by the application of the MSO operator.

In case of carotid CT angiogram it is evident that carotid vasculature and soft/thin bones appear with similar CT intensities. In a CTA data, bone receives high intensity values while contrast enhanced vascular trees appear with intermediate intensity values. Although the intensity characteristics are different for bone and vascular tree, there is a significant overlap between the two due to the presence of partial voluming, noise and soft/thin bones. To evaluate the performance of the MSO operator, CTA data sets were collected using Siemens Somatom Sensation 16 scanner at 120 kV, rotation time of 0.5 second, 0.75 pitch and 0.75 mm collimation. The contrast medium used was 75 cc of Omipaque 300. Bone/vessels separation result using the new MSO operator is illustrated in Fig. 4 (bottom row). The half-skull representation displays the vascular structure in the context of bone geometry.

4 Conclusion

In this paper, the theoretical properties of the multi-scale opening have been established as new mathematical morphological operator. The applicability of the MSO operator has been validated for segmentation of two conjoined fuzzy objects having similar or shared intensity characteristics, which are fused at different scales and locations. The current work extends our previous work [13], [14] on artery-vein separation in 3-D non-contrast pulmonary CT imaging which was formulated as a separation task for two similar-intensity conjoined objects. Qualitative segmentation results of application of the new mathematical morphological operator to mathematical phantoms and artery/vein separation in a physical cast phantom of a pig lung have been illustrated. Elegant segmentation results have been observed from our experiments with the patients' data on non-contrast pulmonary CT and cerebral CTA. High accuracy and reproducibility at the cost of moderate user efforts demonstrates that the new MSO operator is suitable for a wide range of clinical and research studies.

Acknowledgment. Research work of Subhadip Basu is supported by the BOYSCAST fellowship (SR/BY/E-15/09) and FASTTRACK grant (SR/FTP/ETA-04/2012) by DST, Government of India. This study was supported in part by the NIH under Grants R01 AR-054439, R01 HL-083475 and R01 HL-064368. Authors are grateful to Prof. M.L. Raghavan, The University of Iowa and Dr. Robert E. Harbaugh, Penn State Hershey Medical Center for sharing the CTA data used in this study.

References

1. Udupa, J.K., Herman, G.T.: 3D imaging in medicine. CRC Press, Boca Raton (1991)
2. Sonka, M., Hlavac, V., Boyle, R.: Image processing, Analysis, and Machine Vision. Thomson Engineering, Toronto (2007)
3. Sonka, M., Fitzpatrick, J.: Handbook of Medical Imaging: Medical image processing and analysis, vol. 2. SPIE, Bellingham (2000)
4. Bushberg, J.T., Boone, J.M.: The essential physics of medical imaging. Lippincott Williams & Wilkins (2011)
5. Cho, Z.H., Jones, J.P., Singh, M.: Foundations of medical imaging. Wiley, New York (1993)
6. McInerney, T., Terzopoulos, D.: Deformable models in medical image analysis: a survey. Med. Image Anal. **1**, 91–108 (1996)
7. Pham, D.L., Xu, C., Prince, J.L.: Current methods in medical image segmentation 1. Annu. Rev. Biomed. Eng. **2**, 315–337 (2000)
8. Heimann, T., Meinzer, H.-P.: Statistical shape models for 3D medical image segmentation: A review. Med. Image Anal. **13**, 543–563 (2009)
9. Bezdek, J.C., Hall, L.O., Clarke, L.P.: Review of MR image segmentation techniques using pattern recognition. Med. Phys. **20**, 1033 (1993)
10. Olabarriaga, S.D., Smeulders, A.W.M.: Interaction in the segmentation of medical images: A survey. Med. Image Anal. **5**, 127–142 (2001)

11. Saha, P.K., Liang, G., Elkins, J.M., Coimbra, A., Duong, L.T., Williams, D.S., Sonka, M.: A New Osteophyte Segmentation Algorithm Using the Partial Shape Model and Its Applications to Rabbit Femur Anterior Cruciate Ligament Transection via Micro-CT Imaging. Biomed. Eng. IEEE Trans. **58**, 2212–2227 (2011)
12. Van Bemmel, C.M., Spreeuwers, L.J., Viergever, M.A., Niessen, W.J.: Level-set-based artery-vein separation in blood pool agent CE-MR angiograms. IEEE Trans. Med. Imaging **22**, 1224–1234 (2003)
13. Lei, T., Udupa, J.K., Saha, P.K., Odhner, D.: Artery-vein separation via MRA-an image processing approach. IEEE Trans. Med. Imaging **20**, 689–703 (2001)
14. Buelow, T., Wiemker, R., Blaffert, T., Lorenz, C., Renisch, S.: Automatic extraction of the pulmonary artery tree from multi-slice CT data. Medical Imaging, pp. 730–740. International Society for Optics and Photonics (2005)
15. Yonekura, T., Matsuhiro, M., Saita, S., Kubo, M., Kawata, Y., Niki, N., Nishitani, H., Ohmatsu, H., Kakinuma, R., Moriyama, N.: Classification algorithm of pulmonary vein and artery based on multi-slice CT image. Medical Imaging, p. 65142E–65142E. International Society for Optics and Photonics (2007)
16. Saha, P.K., Wehrli, F.W., Gomberg, B.R.: Fuzzy Distance Transform: Theory, Algorithms, and Applications. Comput. Vis. Image Underst. **86**, 171–190 (2002)
17. Rosenfeld, A.: Fuzzy Digital Topology. Inf. Control. **40**, 76–87 (1979)
18. Udupa, J.K., Samarasekera, S.: Fuzzy Connectedness and Object Definition: Theory, Algorithms, and Applications in Image Segmentation. Graph. Model. Image Process. **58**, 246–261 (1996)
19. Saha, P.K., Udupa, J.K.: Iterative relative fuzzy connectedness and object definition: theory, algorithms, and applications in image segmentation. In: Proceedings IEEE Workshop on Mathematical Methods in Biomedical Image Analysis, MMBIA-2000 (Cat. No.PR00737), pp. 28–35. IEEE Comput. Soc.
20. Udupa, J.K., Saha, P.K., Lotufo, R.A.: Relative fuzzy connectedness and object definition: theory, algorithms, and applications in image segmentation. IEEE Trans. Pattern Anal. Mach. Intell. **24**, 1485–1500 (2002)
21. Saha, P.K., Chaudhuri, B.B.: 3D Digital Topology under Binary Transformation with Applications. Comput. Vis. Image Underst. **63**, 418–429 (1996)
22. Saha, P.K., Udupa, J.K.: Optimum image thresholding via class uncertainty and region homogeneity (2001). http://www.computer.org/portal/web/csdl/doi?doc=abs/trans/tp/2001/07/i7toc.htm
23. Otsu, N.: A threshold selection method from gray-level histograms. IEEE Trans. Syst. Man, Cybern. **8**, 62–66 (1978)
24. Kong, T.Y., Rosenfeld, A.: Digital topology: Introduction and survey. Comput. Vis. Graph. Image Process. **48**, 357–393 (1989)
25. Saha, P.K., Chaudhuri, B.B.: Detection of 3-D simple points for topology preserving transformations with application to thinning. Pattern Anal. Mach. Intell. IEEE Trans. **16**, 1028–1032 (1994)
26. Saha, P.K., Wehrli, F.W.: Measurement of trabecular bone thickness in the limited resolution regime of in vivo MRI by fuzzy distance transform. IEEE Trans. Med. Imaging. **23**, 53–62 (2004)
27. Saha, P.K., Udupa, J.K., Odhner, D.: Scale-Based Fuzzy Connected Image Segmentation: Theory, Algorithms, and Validation. Comput. Vis. Image Underst. **77**, 145–174 (2000)
28. Ciesielski, K.C., Udupa, J.K., Saha, P.K., Zhuge, Y.: Iterative Relative Fuzzy Connectedness for Multiple Objects with Multiple Seeds. Comput. Vis. image Underst. CVIU **107**, 160–182 (2007)